Degradation Diagnosis of Power Module Based on Frequency Characteristics in Heat Flow

Mengqi Xu, Ke Ma, *Senior Member, IEEE*, and Quan Zhong

***Abstract*—With the growing demand for highly reliable power electronic systems, the degradation diagnosis of the power modules is becoming increasingly important. Due to its multilayer structure and complex operating conditions, power modules are subject to several different degradation mechanisms and locations. However, most existing approaches for degradation diagnosis are designed to identify only one particular type of degradation. In this article, a novel approach for diagnosing degradations in power modules is proposed based on the frequency-domain heat flow spectrum analysis. Different degradation modes can be clearly distinguished based on the discovery that the frequency-domain heat flow characteristics will change in different frequency bands under different locations of degradation. Simulations and experiments are provided to validate the proposed analysis and method.**

***Index Terms*—Degradation, finite-element method (FEM), frequency domain analysis, power module, reliability.**

I. Introduction

RECENTLY, insulated gate bipolar transistor (IGBT) power modules, have been widely used in reliability-critical and high-power applications such as electric vehicle, wind turbines, smart grids, and power transmission systems [1], [2], where high cost may be paid on maintenances and failures. As a result, it is of great importance for early diagnosis of degradation in power modules to guarantee the safe operation of power electronics.

In practical use, the IGBT power modules are subjected to complicated thermal stresses, including power cycling caused by load variations of mission profiles and thermal cycling cause by variations of surrounding thermal environment [3], [4]. These effects cause cyclic thermo-mechanical stress in all components and joints of the modules [5], leading to fracture initiation and propagation in solders, metallurgical damage to wire bonds and emitter metallization [3], and deterioration of thermal interface material (TIM). Many technologies have been developed for degradation diagnosis in recent years.

Manuscript received 8 January 2023; revised 26 March 2023; accepted 28 April 2023. Date of publication 15 May 2023; date of current version 21 June 2023. This work was supported by the National Nature Science Foundation of China under Grant 52177188. Recommended for publication by Associate Editor O. Lucia. *(Corresponding author: Ke Ma.)*

The authors are with the Key Laboratory of Control of Power Transmission and Conversion, Ministry of Education, Shanghai Jiao Tong University, Shanghai 200240, China, and also with the Department of Electrical Engineering, Shanghai Jiao Tong University, Shanghai 200240, China (e-mail: mengqixu@sjtu.edu.cn; kema@sjtu.edu.cn; zhongquan@sjtu.edu.cn).

Color versions of one or more figures in this article are available at https://doi.org/10.1109/TPEL.2023.3274756.

Digital Object Identifier 10.1109/TPEL.2023.3274756

The method of monitoring thermal resistance is commonly used for detecting solder layer degradation of power modules [6] while electrical parameters like on-state voltage drop $V_{ce(on)}$ for IGBTs are used to evaluate bond wires [7]. Typically, an increase of the internal thermal resistance from the junction to case by 20% or an increase of the $V_{ce(on)}$ by 5% is adopted as the threshold value [8], [9]. Despite its easy implementation, this method has some problems. First, it requires accurate measurement of junction temperature T_j and device's power loss [10]. Normally, thermal sensitive electrical parameters (TSEPs) are applied for T_j [11]. But it requires a comprehensive understanding of the relationship between the TSEPs, device health conditions, and operating conditions [11], making it complicated to be applied in practice. For example, the on-state voltage drop $V_{ce(on)}$ is usually used for estimating T_j [7], but it is also treated as an indicator of the health status of bond wires [12]. However, the degradation of solder layers will also cause increase of T_j and then affect $V_{ce(on)}$ because there is a strong coupling between electrical and thermal characteristics [13]. As a result, it is difficult to identify exactly which degradation happens in power modules.

To deal with these challenges, more advanced methods have been proposed for degradation diagnosis of power modules. A commonly used method is the transient thermal impedance and the structure function as proposed in [14] and [15]. It allows for the diagnosis of different degradation modes by separating the different regions of the internal structure. However, the problem of accurate measuring T_j and power loss still remains. In order to reduce the influence caused by temperature and loss error, another method of extracting the thermal impedance frequency response function (FRF) was proposed in [16] and [17]. It has been discovered that unique changes of phase information in different frequency bands will happen under different degradation modes. But it is difficult to recognize the changing rules from the FRF, so artificial neural networks (ANNs) are recommended for diagnosis of different degradation mechanisms. As a result, massive data is required for training the ANN and the effectiveness of this method cannot be always guaranteed.

Due to the difficulty of monitoring the health status of power module based on T_j, several methods have been developed by utilizing the case temperature T_c, which is easier to be detected. Xiang et al. [8] propose a method of tracking the changes in the case-above-ambient temperature rise and Wang et al. [18] propose a method of using case temperatures measured at two different locations for detecting solder degradation. But these

TABLE I
PARAMETERS FOR THE MATERIAL OF IGBT MODULE

Layers	Material	Thickness d (mm)	Density ρ (kg/m^3)	Thermal conductivity λ (W/m·K)	Specific heat C_p (J/kg·K)
Chip	Si	0.13	2330	148	710
Chip solder	Sn-3.5Ag-0.5Cu	0.08	7500	33	230
Copper	Copper	0.3	8700	395	385
DCB	Al_2O_3	0.38	3750	24	896
Copper	Copper	0.3	8700	395	385
Baseplate solder	Sn-3.5Ag-0.5Cu	0.2	7500	33	230
Baseplate	Copper	3	8700	395	385

techniques normally consider thermal resistance as an indicator for solder layer degradation and ignore the degradation detection for TIM, which is widely used to fill the gaps between the module baseplate and the heatsink in order to improve physical integrity and thermal transfer [6], [19]. As a matter of fact, TIM deterioration is quite common, according to an industry survey [20]. To deal with this issue, Zhang et al. [21] propose an approach to monitor Cauer-type thermal parameters based on the time constants of the case temperature cooling curve, making it possible to simultaneously detect the solder layer degradation and the TIM deterioration. However, all of these methods of using case temperature have one common disadvantage: they are sensitive to the measuring points of the case temperature. For example, it is recommended in [21] that the case temperature sensor be placed directly below the center of the chip, and if there is a deviation of a few millimeters, no degradation will be detected. It severely restricts the application of this technique because there are usually multiple chips in one power module and it is difficult and impractical to install case temperature sensor under each chip.

To overcome the aforementioned concerns and challenges, a novel method of degradation diagnosis of power modules based on the frequency-domain heat flow spectrum has been proposed in this article. It is easy to separate different degradation modes based on the discovery that the frequency-domain heat flow characteristics will change in different frequency bands under different locations of degradation. Furthermore, the effectiveness of the proposed method is independent of the position of the measuring point of the case temperature, providing the possibility of monitoring the health status of multiple chips simultaneously by just setting one case probe. The proposed method is easy to implement and has been verified by both simulations and experiments. It is worth mentioning that the proposed method is effective for degradation diagnosis of the layers which the heat flow passes, such as chip solder and TIM, but not bond wires. Therefore, it is recommended to apply this method in combination with other techniques of detecting the bond wire degradation for complete diagnosis of the power modules in practice.

II. DEGRADATION ANALYSIS OF FREQUENCY-DOMAIN HEAT FLOW SPECTRUM

A novel approach to deal with degradation diagnosis by utilizing the heat flow information under frequency domain is proposed in this article. To study the heat flow characteristics of power modules under frequency domain, a finite-element method (FEM) model needs to be first established.

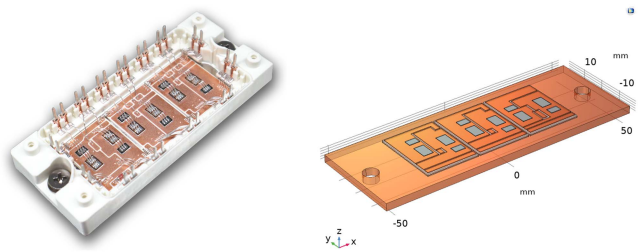

(a) (b)

Fig. 1. Studied IGBT module. (a) Photograph of the module. (b) FEM model built in COMSOL.

A. Power Module and FEM Model Under Study

A 650 V/50 A power module from Starpower with 6 IGBTs and 6 diodes is used as study case in this article, as shown in Fig. 1(a). The parameters for the material of each layer of the studied IGBT module are given in Table I and the construction of the FEM model is illustrated in Fig. 1(b). It should be noted that equivalent heat transfer coefficient (htc) is used as a simplified thermal boundary condition to indicate the heat dissipation capability of the cooling system in this article, and htc = 3000 W/m^2·K is picked as a reference for healthy condition, which is reasonable value for the cooling performance of water-cooled heatsink as stated in [22]. The total mesh of built FEM model has 1 03 269 domain elements, 40 518 boundary elements, and 4794 edge elements.

B. Heat Flow Spectrum of Power Module Under Two Degradation Mechanisms

In order to study the heat flow characteristics under the interested degradation mechanisms, one of the IGBT chips is selected as a boundary heat source and specific locations of measuring points for heat flow nodes are set as shown in Fig. 2, where the measuring point for the junction node is in the center of the studied chip and the case node is allied underneath the chip in the same vertical line. It should be mentioned that point probes are applied to provide the value of heat flux field quantity at these specific points by assuming that the heat flux distribution is assumed to be uniform, so that the characteristics of gain of

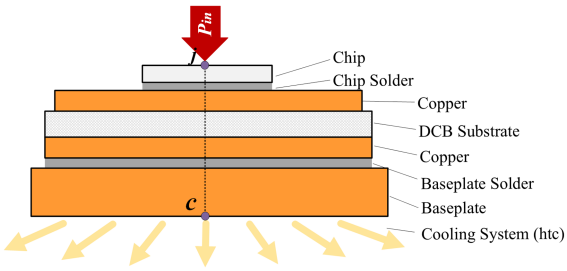

Fig. 2. Locations of the probes for heat flow characteristics during FEM simulation.

heat flow can be seen as the same as heat flux

$$G_{P_{in}P_{out}}(s) \approx G_{q_j q_c}(s) \tag{1}$$

where P refers to heat flow and q refers to heat flux.

Then, a two-step simulation is conducted to obtain heat flow spectrum $G_{P_{in}P_{out}}(s)$: the first step is a stationary study step which computes the stationary/bias solution; the second step is the frequency domain perturbation step, which computes a perturbed solution of the linearized problem around the linearization point (or bias point) computed in the first step [23].

Many studies indicate that the cyclic thermo-mechanical stress caused by complicated operating profiles in all components and joints of the modules [5] leads to crack, void, and delamination in the different interface layers [21], [24], especially the chip solder. Therefore, chip solder degradation is studied in detail. Besides, the TIM deterioration is also an important issue because the TIM is also tended to failure when subjected to a wide range of cyclic thermal-mechanical stresses, and the failure of TIM is primarily due to grease pump-out and dry-out [25]. The TIM deterioration causes an increase in thermal resistance, leading to over-heating of the power modules. As a result, the influences of TIM deterioration on heat flow characteristics under frequency domain is also important, which should be carefully studied.

1) Chip Solder Degradation: Prior research, including FEM simulation and experimental X-ray images, demonstrated that solder degradation initiates from the edges and propagates inward to the center [19], along with voids that range in size from 10 to 150 μm randomly distributed in various shapes [26]. As a result, to simulate the degradation happened in the chip solder layer by FEM, it is assumed that the area of chip solder is reduced and the crack grows from edge toward the center point of this layer [18], [19]. As well as the crack growth with the increase of degradation degree, voids with different sizes are added in chip solder layer [4], [26], [27], which makes the simulation results close to the real situation. As shown in Fig. 3, six conditions are considered here and the remained area of the chip solder layer under each condition is also indicated.

Repeated frequency-domain FEM simulations with the six different conditions in Fig. 3 are thereby conducted. For each case, a two-step simulation as mentioned above is required and the changes of heat flow spectrum $G_{P_{in}P_{out}}(s)$ with the decrease

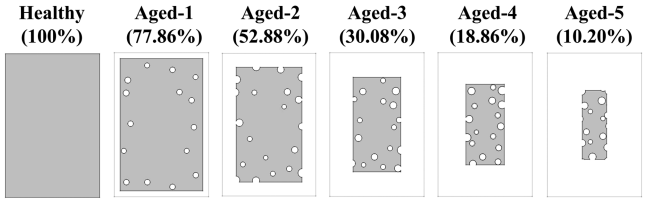

Fig. 3. Six conditions of the health status of chip solder in FEM simulation.

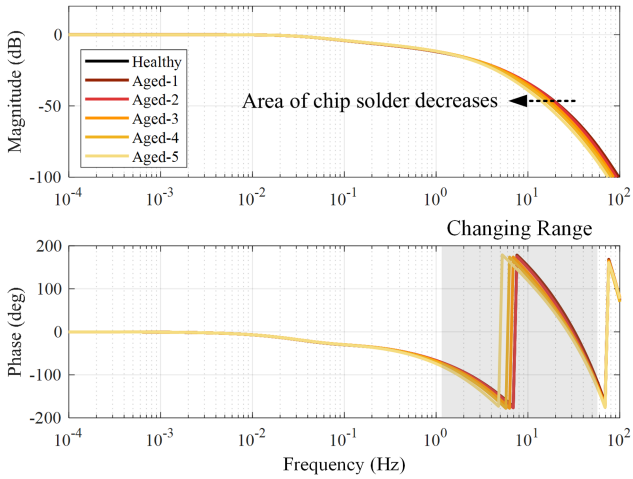

Fig. 4. Heat flow characteristics in frequency domain with different sizes of chip solder layer.

of area of chip solder can be obtained as illustrated in Fig. 4. It can be seen that, as the area of chip solder decreases, the magnitude plot of heat flow tends to decay more quickly, and the phase plot that the frequency band from 1 to 50 Hz is significantly influenced when degradation happens in the layer of chip solder.

2) TIM Deterioration: In addition to solder degradation, TIM deterioration is also very common in power modules, so how the heat flow spectrum changes when TIM deterioration happens is an important issue. In COMSOL, the equivalent htc of the cooling system is used to indicate the amount of heat transported between a solid and a fluid by convection in order to represent the cooling system's capacity [22].

According to the existing research in [6] and [21], TIM degradation causes an increase in thermal resistance and a reduction in heat dissipation performance. As a result, TIM deterioration can be simulated by reducing the value of htc in FEM simulation, are shown in Fig. 5, where the variation of heat flow spectrum $G_{P_{in}P_{out}}(s)$ is presented. It can be seen that the magnitude plot of heat flow also begins to decay at a much lower frequency band as htc reduces, and the frequency band from 10^{-3} to 10^{-1} Hz of the phase plot is mainly influenced.

As a conclusion, frequency-domain heat flow characteristics will change in different frequency bands under two locations of degradation. But it is not obvious by just observing the bode plots of heat flow, thereby a novel approach to diagnose degradation will be demonstrated in the next section.

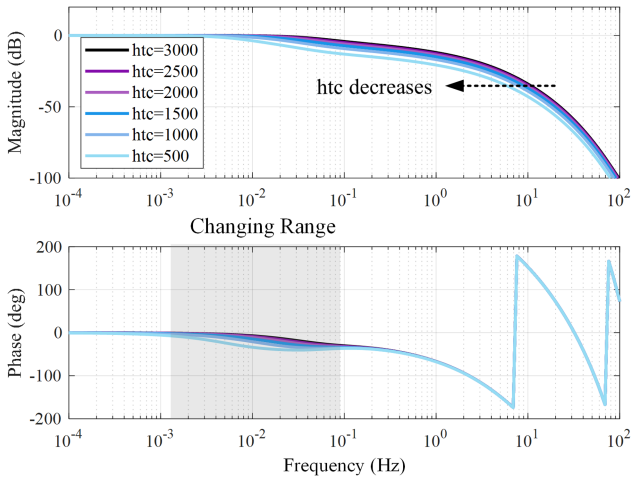

Fig. 5. Heat flow characteristics in frequency domain with different htcs.

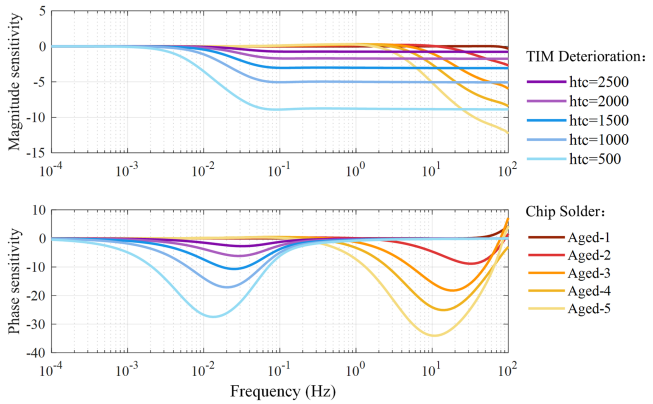

Fig. 6. Bode plot of the normalized sensitivity function for different degradation mechanisms.

III. Proposed Method for Degradation Diagnosis

A. Sensitivity Function

To better distinguish different degradation mechanisms, a normalized sensitivity function S is defined here as the ratio of an aged power module's heat flow transfer function to the original heat flow transfer function of a healthy power module

$$S_{Aged-i}(s) = \frac{G^{Aged-i}_{P_{in}P_{out}}(s)}{G^{Heatlhy}_{P_{in}P_{out}}(s)} \tag{2}$$

where s is the Laplace operator and i refers to each condition of different aging degrees.

The bode plot of the normalized sensitivity function is shown in Fig. 6, and it is easy to identify different degradation mechanisms from the phase information. When chip solder degradation happens, the frequency band around 10 Hz has a great deviation from the origin. When TIM degradation occurs, there is a significant departure from origin in the frequency range around 0.01 Hz.

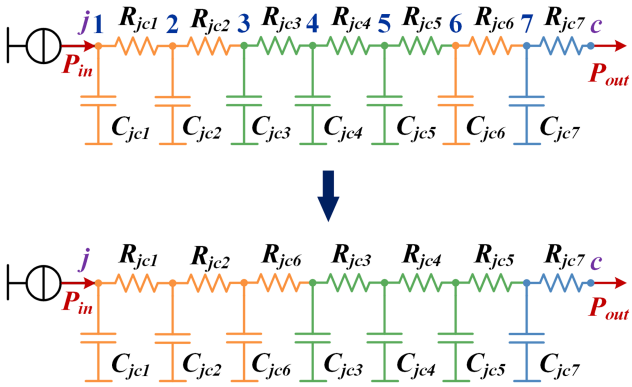

Fig. 7. Principle of constructing LPF for heat flow.

B. Heat Flow Function of Power Module Under Frequency Domain

As can be seen in Figs. 4 and 5, the frequency-domain heat flow from chip to case node behaves like a low-pass filter (LPF). The principle of constructing the LPF is shown in Fig. 7, which assumes that a 7-layer Cauer network can be used for describing the thermal behavior of the power module. Thus, the heat flow through each internal layer within the power module behaves as first-order LPFs. Also, it was found that certain heat flow gains exhibit similarities and can be grouped together. As a result, a 7order-3frequencies LPF has been proposed to describe the LPF characteristics of heat flow from junction to case in our previous work [28]

$$G_{LPF}(s) = \left(\frac{2\pi f_1}{s+2\pi f_1}\right)^1 \left(\frac{2\pi f_2}{s+2\pi f_2}\right)^3 \left(\frac{2\pi f_3}{s+2\pi f_3}\right)^3 \tag{3}$$

where f_1, f_2, and f_3 are the critical frequencies of the LPF, and s is the Laplace operator. The three critical frequencies satisfy $f_1 < f_2 < f_3$, and each parameter its explicit mathematical and physical meaning: f_1 corresponds to low frequency band composed of baseplate layer, f_2 corresponds to medium frequency band composed of the DCB layer and two copper layers, and f_3 corresponds to high frequency band composed of chip layer and two solder layers.

By using the parameter extraction method in our previous work proposed in [29], the three critical frequencies of LPF are identified as $f_1 = 0.2235$, $f_2 = 16.5$, and $f_3 = 81.39$ Hz for the healthy power module, respectively. To prove the effectiveness of the aforementioned LPF with the identified parameters, Fig. 8 compares the bode plot of identified LPF with FEM results, showing that the identified LPF is highly consistent with simulation results below 100 Hz. It is important to note that FEM results suggest that the LPF should have a higher order, but for the sake of simplifying the modeling process, a seventh-order LPF is used here. This is reasonable because the magnitude of the heat flow is below -100 dB in the frequency band above 100 Hz, indicating that some high-frequency thermal behaviors can be neglected.

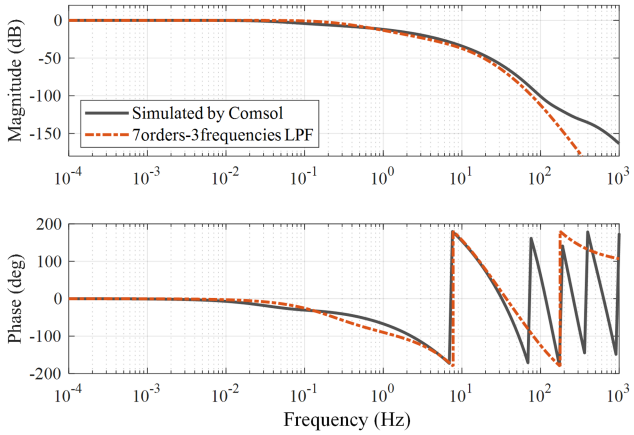

Fig. 8. Comparison of extracted 7order-3frequencies LPF with FEM results of heat flow characteristics under frequency domain.

C. Impacts on Critical Frequencies of LPF With Different Degradations

With the information of the proposed 7order-3frequencies LPF structure, the characteristics of heat flow in different frequency bands when different modes of degradation occur can be studied. Corresponding to the range of frequency band influenced by the two degradation mechanisms illustrated in Fig. 6, it can be deduced that f_1 will be influenced when solder degradation happens, while f_2 will be influenced when TIM deterioration happens. But the changing trend should be studied in detail and the parameters of LPF under each case can be easily obtained using the aforementioned parameter extraction method.

When TIM deterioration happens, the lowest critical frequency f_1 of the 7order-3frequencies LPF represented in (3) is the only parameter that influenced by the variation of htc, and its changing trend is illustrated in Fig. 9(a). It demonstrates that as the decrease of heat transfer capability of cooling system, f_1 decreases.

Similarly, when chip solder degradation happens, it is obvious in the phase plot of Fig. 6 that the frequency band around 10 Hz is significantly influenced. As a result, only the medium critical frequency f_2 in the LPF is supposed to be smaller when chip solder degradation happens, and the identified f_2 under each case of Fig. 3 is shown in Fig. 9(b). It can be concluded that as the remained area of chip solder decreases, f_2 decreases.

As for the highest critical frequency, f_3, is noted to correspond to a high frequency band around 100 Hz, and this frequency will not change in the types of degradation studied in this article. As a result, the deviation of f_3 is not considered.

It can be concluded that frequency bands influenced by degradation are slightly different from the critical frequency represented for corresponding layer in LPF. For example, the chip solder layer should correspond to f_3, which is 81.39 Hz, but when the chip solder layer degrades, the frequency band around 10 Hz is mainly affected, thus affecting f_2. Fortunately, although it is difficult to establish a one-to-one correspondence, there is a certain regularity that the frequency bands that undergo

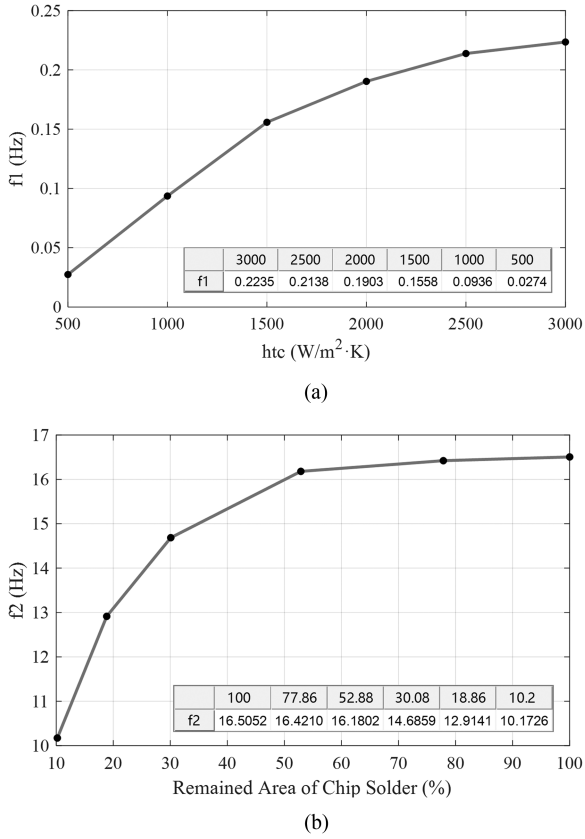

Fig. 9. Changing trend of LPF parameters when degradation happens. (a) f_1 with different htcs. (b) f_2 with different remained areas of chip solder.

changes are about ten times smaller than the critical frequencies. Therefore, the critical frequency f_1 and f_2 can be picked as the indicator of TIM deterioration and chip solder degradation, respectively. This regularity can be applied for different modules and the LPF can be expressed in a more general form

$$G_{LPF}(s) = \left(\frac{2\pi f_1}{s+2\pi f_1}\right)^a \left(\frac{2\pi f_2}{s+2\pi f_2}\right)^b \left(\frac{2\pi f_3}{s+2\pi f_3}\right)^c \quad (4)$$

where $a+b+c=N$. N refers to the number of layers inside power module. The order of each critical frequency depends on the grouping classification, as illustrated in Fig. 7.

In a conclusion, the critical frequency f_1 and f_2 of LPF can be picked as the indicator of degradation. But it is still difficult to establish a universal standard for defining the degree of degradation because the rate of change in critical frequencies for different power modules may vary, and it requires further research.

D. Experimental Validation of TIM Deterioration

Since htc is a simplified representation of boundary condition in simulations, the study of TIM deterioration by reducing htc in FEM is not much close to the real situation. Therefore, it is necessary to conduct experiments to uncover the changing trend of f_1 when TIM deterioration happens.

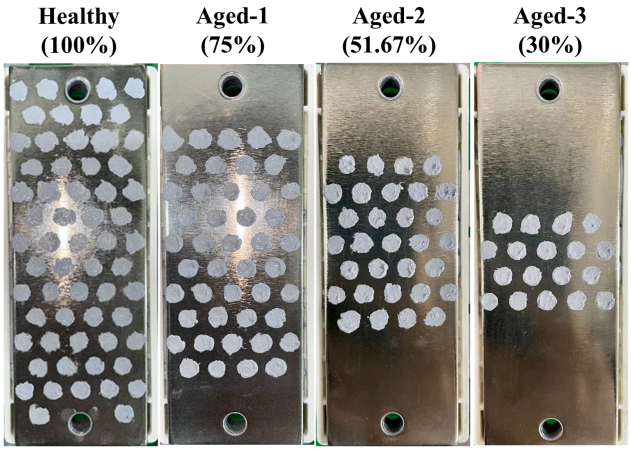

Fig. 10. Four conditions of thermal grease for studying TIM deterioration.

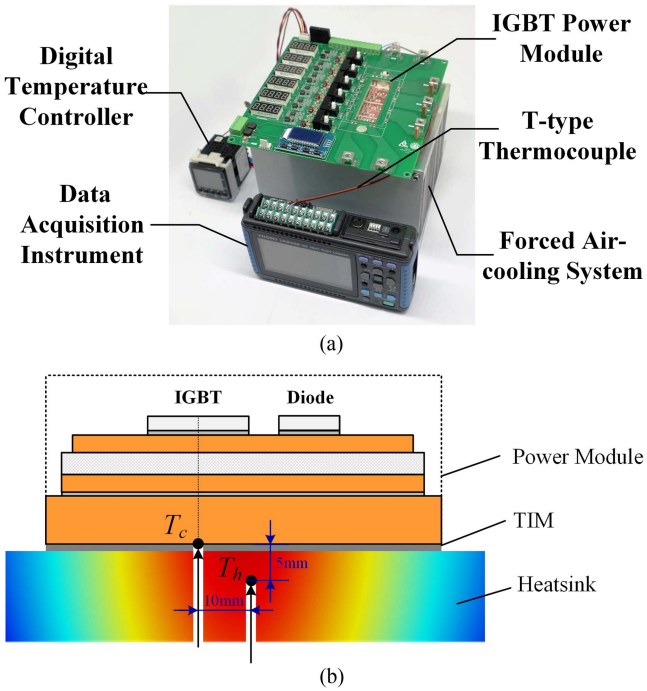

Fig. 11. Experimental setup. (a) Photograph of the experimental setup. (b) Locations of case and heatsink temperature sensors.

In order to simulate TIM deterioration, four conditions of thermal grease are considered here as shown in Fig. 10. It can be estimated that the remained area of TIM for four conditions are 100%, 75%, 51.67%, and 30%, respectively. Then, the change of the lowest critical frequency f_1 should be studied.

However, in practice, it is difficult to directly measure heat flow behaviors to identify the parameters of LPF. As a result, the method of obtaining LPF parameters by indirect approach through the difference of case and heatsink temperature nodes ΔT_{ch} (t) is adopted. The experimental setup is shown in Fig. 11(a) and T-type thermocouples (omega TJC36-CPSS-020G-2) with the accuracy of ± 1 °C and the response time of 0.1 s are applied for temperature measurement. The detail

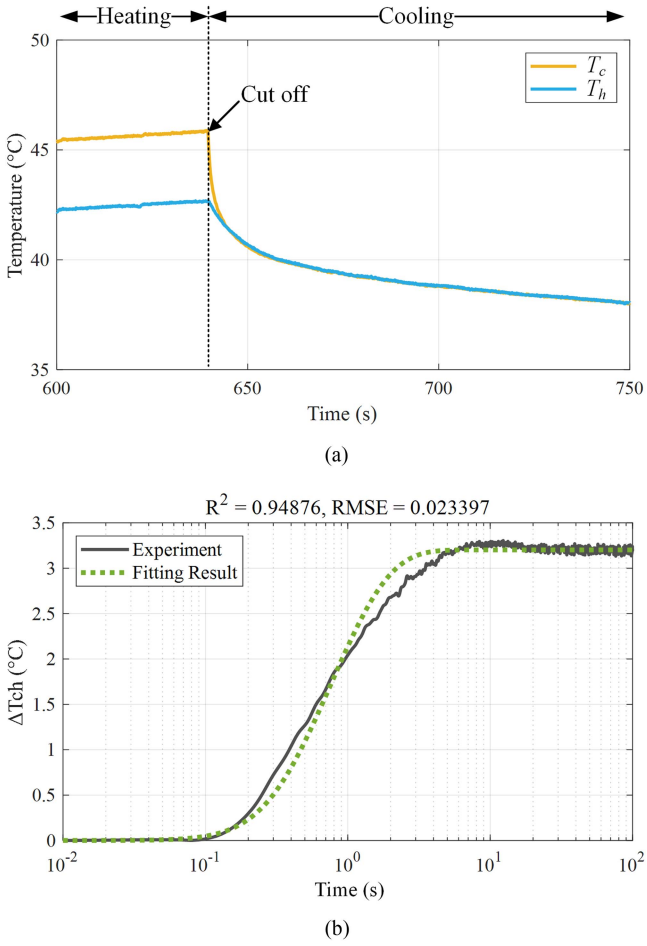

Fig. 12. Curves of condition of Aged-1 in Fig. 10. (a) Experimental temperature curves for case and heatsink with heating current of 30 A. (b) Comparison of fitting results of ΔT_{ch} during cooling phase with experiment.

explanation of the method by using ΔT_{ch} (t) has been stated in [28] and it has been discovered that the parameters of LPF can be accurately obtained if the two temperature sensors for case and heatsink are close enough. The locations of case and heatsink sensors for calculating ΔT_{ch} (t) are illustrated in Fig. 11(b), which satisfy the requirement that the case sensor is close to heatsink sensor. Furthermore, all the temperature curves are measured during cooling phase according to the JEDEC Standard [30].

Take the condition of Aged-1 as an example, Fig. 12(a) shows the experimental curves of case and heatsink with heating current of 30 A in this case. The ΔT_{ch} (t) curve is calculated after cutting off the heating current. Then, by using the parameter extraction method of our previous work in [29], the LPF parameters under each case can be obtained. Fig. 12(b) illustrates the fitting result of Aged-1, which has a good agreement with experiment with 0.94876 of R^2, proving the effectiveness of the parameter extraction method and the high accuracy of obtained parameters.

Therefore, the parameter of LPF for each condition can be obtained as shown in Fig. 13. It should be noted that the lowest critical frequency f_1 will be influenced when TIM deterioration happens, so only the changing trend of f_1 with the reduction of

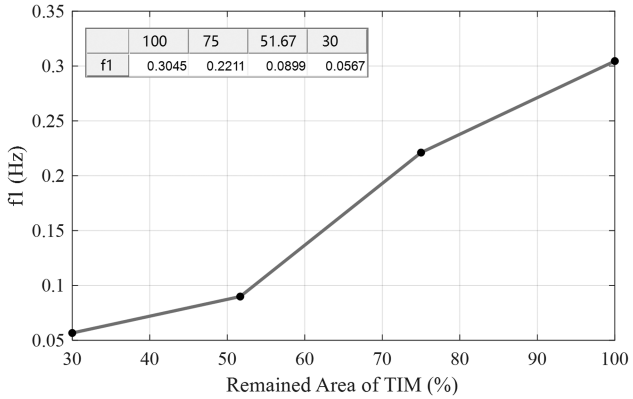

Fig. 13. Identified f_1 under four conditions of TIM in Fig. 10.

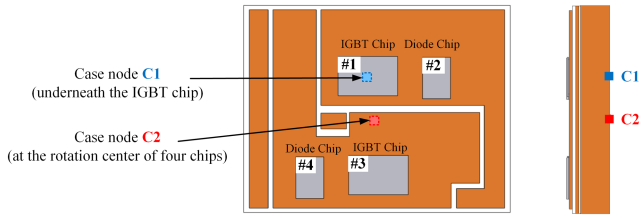

Fig. 14. Two positions of case node.

area of TIM is taken into account in Fig. 13. It is evident that as the degree of TIM degradation increases, f_1 decreases, consistent with the simulation results. As a result, the TIM degradation can be diagnosed by the proposed method of monitoring f_1: when f_1 is decreased to some degree, there might TIM degradation happens and it is recommended to concern the health status of TIM.

As a conclusion, the heat flow characteristics in the frequency domain under different degradation mechanisms are studied in this section. The proposed method by using the frequency-domain heat flow spectrum for diagnosis of degradation that occur in power modules is verified by FEM simulations and experiments.

IV. Influence of Case Node Position

One power module typically contains several chips, making it inconvenient to place a case temperature sensor under each chip. Thus, the measuring point for case is not always set right underneath the interested chip. But for existing methods, for example, the method of [21], the temperature sensor should be placed directly below the center of the chip to ensure its effectiveness, severely limiting its application. As a result, the influence of case node position on the proposed method should be carefully studied and FEM simulations are conducted first.

A. FEM Simulation

In FEM simulations, two positions of case nodes are considered as shown in Fig. 14. Case node C1 in blue is set underneath the IGBT chip, while case node C2 in red is set at the rotation center of four chips in the same DCB section.

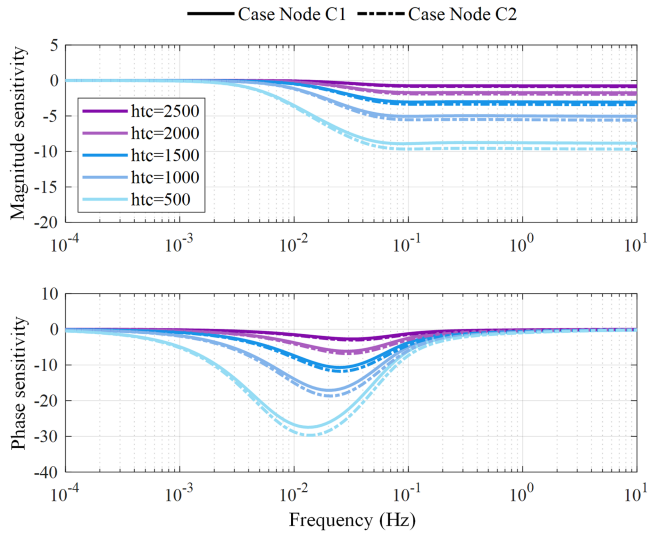

Fig. 15. Bode plot of the normalized sensitivity function for two case nodes with different htcs.

TABLE II
Identified LPF Parameters for Different htcs With Two Case Nodes

htc	Case node C1		Case node C2	
	f_l (Hz)	Δf_l	f_l (Hz)	Δf_l
3000	0.2235	0	0.1704	0
2500	0.2138	−4.34%	0.1602	−5.96%
2000	0.1903	−14.85%	0.1426	−16.31%
1500	0.1558	−30.29%	0.1138	−33.22%
1000	0.0936	−58.12%	0.0678	−60.21%
500	0.0274	−87.74%	0.0184	−89.20%

The comparison of sensitivity function for two case nodes is shown in Fig. 15, where TIM deterioration is simulated. It can be seen that the bode plot of sensitivity function for C2 as case node is almost the same as that of C1. It means that position of case node brings little influence on the effectiveness of the proposed method for degradation diagnosis of power modules, but quantitative analysis is also required for better understanding. Therefore, the changing trend of f_1 should be studied by selecting C2 as case node and the rate of change in f_1 is defined to uncover the degree of impact

$$\Delta f_{1,i} = \frac{f_{1,i} - f_{1,htc=3000}}{f_{1,htc=3000}} \times 100\% \tag{5}$$

where i refers to each condition of htc varied from 2500 to 500.

As can be seen in Table II, the parameters f_1 for two case nodes under the same TIM condition are different but the changing trends of f_1 are the same: f_1 decreases with the decrease of htc. Also, the rates of change in f_1 calculated in (5) are shown in Fig. 16, indicating that the degradation degree detected with case node C1 is much close to those with case node C2. To verify this conclusion, experiments are also provided as follows.

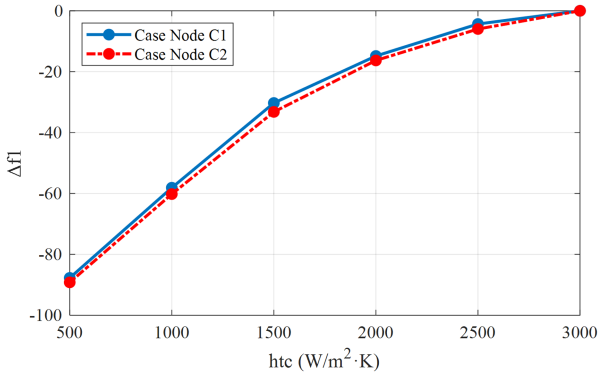

Fig. 16. Comparison of two case nodes when htc varies from 3000 to 500 W/m^2·K by Δf_1.

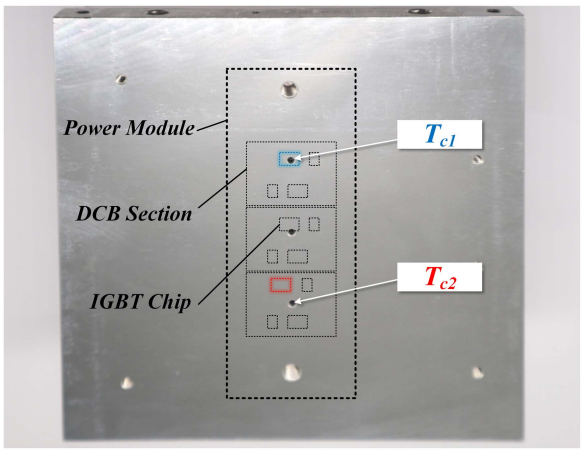

Fig. 17. Locations of temperature sensors.

B. Experimental Verification

For experiments, two different positions of measuring point of case temperature are applied as shown in Fig. 17, T_{c1} is set right underneath the IGBT chip in red and T_{c2} is set several millimeters away from the IGBT chip in blue. For each case sensor, the corresponding heatsink temperature sensor, is close enough in order to reduce errors caused by measurement and the distance is shown in Fig. 11(b).

In the previous section, all the experiments are carried out by measuring T_{c1}, so four additional experiments of different TIM conditions are carried out by choosing T_{c2} as the case temperature. Similarly, by using the parameter extraction method of by utilizing $\Delta T_{ch}(t)$ proposed in our previous work in [29], the LPF parameters under each case by selecting T_{c2} can be obtained and the comparison of two nodes are shown in Fig. 18 and the corresponding parameters are listed in Table III. It is evident that this proposed approach is applicable regardless of the case node's position that the change rates of f_1 in each condition of two nodes are almost the same.

As a result, it can be concluded that the effectiveness of the proposed approach does not depend on where the case node is located. This means that users have a large amount of flexibility in deciding where to place the case probe. From a different angle,

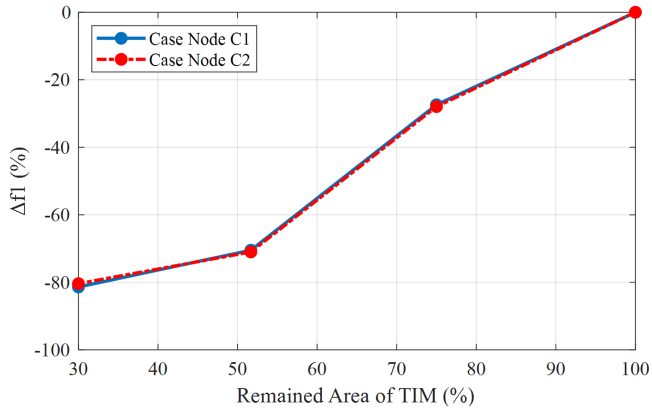

Fig. 18. Comparison of two case nodes in experiments by Δf_1.

TABLE III
IDENTIFIED LPF PARAMETERS FOR DIFFERENT TIM CONDITIONS WITH TWO CASE NODES IN EXPERIMENTS

Condition	Case node C1		Case node C2	
	f_1 (Hz)	Δf_1	f_1 (Hz)	Δf_1
Healthy (100%)	0.3045	0	0.2472	0
Aged-1 (75%)	0.2211	−27.39%	0.1781	−27.95%
Aged-2 (51.67%)	0.0899	−70.48%	0.0717	−71.00%
Aged-3 (30%)	0.0567	−81.38%	0.0485	−80.38%

it provides the possibility of setting just one case node to monitor the health status of multiple chips. For instance, by positioning the rotation center C2 of four chips in the same DCB section as the case node, it is convenient to monitor the health status of each chip.

V. LIMITATIONS AND DISCUSSIONS

A. Chip Solder Degradation

As a matter of fact, the accuracy of extracted LPF parameters is highly dependent on the bandwidth of measurement. Take the temperature sensors of T-type thermocouples for applied in this article as an example, the response time of sensors is limited at 0.1 s, i.e., the recorded temperature data are invalid before 0.1 s, corresponding to a cut-off frequency of 1.6 Hz. Then, the thermal behavior over 1.6 Hz will be filtered out and only the accuracy of critical frequencies below 1.6 Hz can be guaranteed. As a result, it is difficult to detect high-frequency band degradation, like chip solder degradation, by using the temperature sensors of this article. However, this problem can be solved if advanced measuring instrument with higher accuracy and faster response time appear in the future.

B. Baseplate Solder Degradation

There are two solder joints in a power module: the Si chip – DCB solder joint and the DCB – baseplate solder joint [31]. The previous sections studied chip solder degradation in depth, whereas baseplate solder degradation is ignored. Similar to the settings of simulating chip solder degradation, the baseplate solder degradation is simulated by four conditions of 100%,

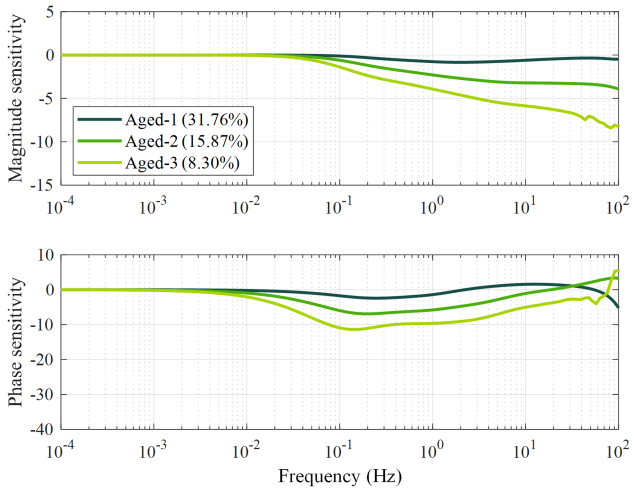

Fig. 19. Heat flow characteristics in frequency domain with different sizes of baseplate solder layer.

31.76%, 15.87%, and 8.30% of original baseplate solder area, respectively. The FEM results of frequency domain heat flow behaviors can be thereby obtained and the bode plots of sensitivity function for each aging case are depicted in Fig. 19. But there are mainly two problems that worth mentioning: First, the phase plot shows that the frequency band from 10^{-2} to 10^{1} Hz is influenced when baseplate solder degradation happens, which is much wider than those of chip solder degradation and TIM deterioration. Second, the heat flow spectrum is insensitive to baseplate solder degradation that only small changes are detected when the remained area of baseplate solder is very small. For example, little influence can be detected when the remained area of baseplate solder is reduced to 31.76% of origin. As a result, the critical frequencies of LPF are supposed not to change greatly when baseplate solder degradation happens, and the variation of critical frequencies can even be ignored. A possible reason could be that the area of the baseplate solder layer is significantly larger than that of the chip solder layer. Therefore, the diffusion process of heat transfer from the chip, acting as a heat source, is less affected by the degradation of the baseplate solder layer.

As a result, it is still a difficult problem for detecting degradation of baseplate solder by the proposed method in this article, and it requires further research.

VI. Conclusion

This article proposes a novel approach by studying the frequency-domain heat flow spectrum for diagnosis of different degradation mechanisms that occur in power modules. By monitoring the LPF parameters, it is easy to identify the degradation mode because the frequency-domain heat flow characteristics will change in different frequency bands under different locations of degradation. Two degradation mechanisms have been thoroughly investigated and it has been discovered that the high-frequency band heat flow behaviors are influenced when solder degradation happens while the low-frequency band heat flow behaviors are significantly influenced when TIM deterioration happens. Compared with existing methods, the main advantage of the proposed method is that its sensitivity is independent on the position of case node, making it easy to implement in practice. The proposed method has been validated by both simulated and experimental results.

References

[1] F. Blaabjerg and K. Ma, "Future on power electronics for wind turbine systems," *IEEE J. Emerg. Sel. Topics Power Electron.*, vol. 1, no. 3, pp. 139–152, Sep. 2013, doi: 10.1109/JESTPE.2013.2275978.

[2] W. Wang, K. Ma, and X. Cai, "Efficient capacitor voltage balancing method for modular multilevel converter under carrier-phase-shift pulsewidth modulation," *IEEE Trans. Power Electron.*, vol. 36, no. 2, pp. 1553–1562, Feb. 2021, doi: 10.1109/TPEL.2020.3009272.

[3] V. Smet et al., "Ageing and failure modes of IGBT modules in high-temperature power cycling," *IEEE Trans. Ind. Electron.*, vol. 58, no. 10, pp. 4931–4941, Oct. 2011, doi: 10.1109/TIE.2011.2114313.

[4] M. Ciappa, "Selected failure mechanisms of modern power modules," *Microelectronics Rel.*, vol. 42, no. 4–5, pp. 653–667, Apr. 2002, doi: 10.1016/S0026-2714(02)00042-2.

[5] N. Kaminski, E. Özkol, S. Hartmann, and H. Duran, "Load-cycling capability of HiPak IGBT modules," ABB Application note, 2012. [Online]. Available: http://www05.abb.com/global/scot/scot256.nsf/veritydisplay/ec2cf0cf56cf47e8c1257a02002776e1/$file/5SYA2043-03May12(Load-cyclingcapabilityofHiPakIGBTmodules).pdf

[6] J. Cai, L. Zhou, P. Sun, T. Zhou, and Q. Li, "Effect of TIM deterioration on monitoring of IGBT module thermal resistance and its compensation strategy," *IEEE Trans. Compon., Packag., Manuf. Technol.*, vol. 12, no. 5, pp. 789–797, May 2022, doi: 10.1109/TCPMT.2022.3169156.

[7] B. Ji, V. Pickert, W. Cao, and B. Zahawi, "In situ diagnostics and prognostics of wire bonding faults in IGBT modules for electric vehicle drives," *IEEE Trans. Power Electron.*, vol. 28, no. 12, pp. 5568–5577, Dec. 2013, doi: 10.1109/TPEL.2013.2251358.

[8] D. Xiang, L. Ran, P. Tavner, A. Bryant, S. Yang, and P. Mawby, "Monitoring solder fatigue in a power module using case-above-ambient temperature rise," *IEEE Trans. Ind. Appl.*, vol. 47, no. 6, pp. 2578–2591, Nov./Dec. 2011, doi: 10.1109/TIA.2011.2168556.

[9] PC and TC Diagrams, Infineon Application Note AN2019-05, 2019. [Online]. Available: https://www.infineon.com/dgdl/Infineon-AN2019-05_PC_and_TC_Diagrams-ApplicationNotes-v02_01-EN.pdf?fileId=5546d46269e1c019016a594443e4396b

[10] J. Zhang, X. Du, W. Xiao, and S. Zheng, "Condition monitoring the health status of forced air cooling system using the natural frequency of thermal network," *IEEE Trans. Power Electron.*, vol. 34, no. 11, pp. 10408–10413, Nov. 2019, doi: 10.1109/TPEL.2019.2923801.

[11] N. Baker, M. Liserre, L. Dupont, and Y. Avenas, "Improved reliability of power modules: A review of online junction temperature measurement methods," *IEEE Ind. Electron. Mag.*, vol. 8, no. 3, pp. 17–27, Sep. 2014, doi: 10.1109/MIE.2014.2312427.

[12] R. Schmidt, U. Scheuermann, S. E. Gmbh, and C. Kg, "Separating failure modes in power cycling tests," in *Proc. 7th Int. Conf. Integr. Power Electron. Syst.*, 2012, pp. 1–6.

[13] Y. Jia, Y. Huang, F. Xiao, H. Deng, Y. Duan, and F. Iannuzzo, "Impact of solder degradation on VCE of IGBT module: Experiments and modeling," *IEEE J. Emerg. Sel. Topics Power Electron.*, vol. 10, no. 4, pp. 4536–4545, Aug. 2022, doi: 10.1109/JESTPE.2019.2928478.

[14] V. Szbkely and T. van Bien, "Fine structure of heat flow path in semiconductor devices: A measurement and identification method," *Solid State Electron.*, vol. 31, no. 9, pp. 1363–1368, 1988.

[15] V. Szekely, S. Torok, E. Nikodemusz, G. Farkas, and M. Rencz, "Measurement and evaluation of thermal transients," in *Proc. 18th IEEE Instrum. Meas. Technol. Conf. Rediscovering Meas. Age Inform.*, 2002, vol. 1, pp. 210–215. doi: 10.1109/IMTC.2001.928814.

[16] C. H. van der Broeck, S. Kalker, T. A. Polom, R. D. Lorenz, and R. W. de Doncker, "In-situ thermal impedance spectroscopy of power electronic modules for localized degradation identification," in *Proc. Int. Exhib. Conf. Power Electron., Intell. Motion, Renewable Energy, Energy Manage.*, 2019, pp. 1097–1104.

[17] C. H. van der Broeck, T. A. Polom, and R. W. de Doncker, "Diagnosing power module degradation with high-resolution, data-driven methods," in *Proc. IEEE Energy Convers. Congr. Expo.*, 2021, pp. 3607–3614, doi: 10.1109/ECCE47101.2021.9594921.

[18] Z. Wang, W. Qiao, and L. Qu, "A real-time adaptive IGBT thermal model based on an effective heat propagation path concept," *IEEE J. Emerg. Sel. Topics Power Electron.*, vol. 9, no. 4, pp. 3936–3946, Aug. 2021, doi: 10.1109/JESTPE.2020.2973181.

[19] B. Ji et al., "In situ diagnostics and prognostics of solder fatigue in IGBT modules for electric vehicle drives," *IEEE Trans. Power Electron.*, vol. 30, no. 3, pp. 1535–1543, Mar. 2015, doi: 10.1109/TPEL.2014.2318991.
[20] K. Fischer, T. Stalin, H. Ramberg, J. Wenske, and R. Karlsson, "Investigation of converter failure in wind turbines," *Elforsk*, vol. 58, no. 12, 2012, Art. no. 69.
[21] J. Zhang, X. Du, Y. Wu, Q. Luo, P. Sun, and H.-M. Tai, "Thermal parameter monitoring of IGBT module using case temperature," *IEEE Trans. Power Electron.*, vol. 34, no. 8, pp. 7942–7956, Aug. 2019, doi: 10.1109/TPEL.2018.2879825.
[22] A. S. Bahman, K. Ma, and F. Blaabjerg, "A lumped thermal model including thermal coupling and thermal boundary conditions for high-power IGBT modules," *IEEE Trans. Power Electron.*, vol. 33, no. 3, pp. 2518–2530, Mar. 2018, doi: 10.1109/TPEL.2017.2694548.
[23] "COMSOL multiphysics reference manual," in *COMSOL Multiphysics v. 5.5*, Stockholm, Sweden, 2018. [Online]. Available: https://doc.comsol.com/5.5/docserver/#!/com.comsol.help.comsol/html_COMSOL_ReferenceManual.html
[24] M. Bouarroudj, Z. Khatir, J.-P. Ousten, and S. Lefebvre, "Temperature-level effect on solder lifetime during thermal cycling of power modules," *IEEE Trans. Device Mater. Rel.*, vol. 8, no. 3, pp. 471–477, Sep. 2008, doi: 10.1109/TDMR.2008.2002354.
[25] I. M. Nnebe and C. Feger, "Drainage-induced dry-out of thermal greases," *IEEE Trans. Adv. Packag.*, vol. 31, no. 3, pp. 512–518, Aug. 2008, doi: 10.1109/TADVP.2008.924231.
[26] A. Surendar, L. G. Akhmetov, L. K. Ilyashenko, A. Maseleno, and V. Samavatian, "Effect of thermal cycle loadings on mechanical properties and thermal conductivity of a porous lead-free solder joint," *IEEE Trans. Compon., Packag., Manuf. Technol.*, vol. 8, no. 10, pp. 1769–1776, Oct. 2018, doi: 10.1109/TCPMT.2018.2861777.
[27] D. C. Katsis and J. D. van Wyk, "Void-induced thermal impedance in power semiconductor modules: Some transient temperature effects," *IEEE Trans. Ind. Appl.*, vol. 39, no. 5, pp. 1239–1246, Sep./Oct. 2003, doi: 10.1109/TIA.2003.816527.
[28] M. Xu, K. Ma, Q. Zhong, and M. Liserre, "Frequency-domain thermal modeling of power modules based on heat flow spectrum analysis," *IEEE Trans. Power Electron.*, vol. 38, no. 2, pp. 2446–2455, Feb. 2023, doi: 10.1109/TPEL.2022.3210505.
[29] K. Ma, M. Xu, and B. Liu, "Modeling and characterization of frequency-domain thermal impedance for IGBT module through heat flow information," *IEEE Trans. Power Electron.*, vol. 36, no. 2, pp. 1330–1340, Feb. 2021, doi: 10.1109/TPEL.2020.3009257.
[30] *Transient Dual Interface Test Method for the Measurement of the Thermal Resistance Junction to Case of Semiconductor Devices with Heat Flow Through a Single Path*. JEDEC Standard JESD51-14, 2010.
[31] C. Busca et al., "An overview of the reliability prediction related aspects of high power IGBTs in wind power applications," *Microelectronics Rel.*, vol. 51, no. 9–11, pp. 1903–1907, Sep. 2011, doi: 10.1016/j.microrel.2011.06.053.

Mengqi Xu received the B.Sc. degree in electrical engineering from Nanjing University of Aeronautics and Astronautics, Nanjing, China, in 2018. She is currently working toward the Ph.D. degree in electrical engineering with Shanghai Jiao Tong University, Shanghai, China.

Her research interests include the thermal modeling and reliability analysis of power electronics.

Ke Ma (Senior Member, IEEE) received the B.Sc. and M.Sc. degrees in electrical engineering from Zhejiang University, Hangzhou, China, in 2007 and 2010, respectively, and the Ph.D. degree in electrical engineering from Aalborg University, Aalborg, Denmark, in 2013.

In 2014, he became an Assistant Professor with Aalborg University. In 2016, he joined the Faculty of Shanghai Jiao Tong University, China, and is currently a Tenured Associate Professor, he is meanwhile serving as the Deputy Director for the Key Laboratory of Control of Power Transmission and Conversion, Ministry of Education, China. His current research interests include the power electronics and its reliability in the application of renewable energy, HVdc, and motor drive systems.

Dr. Ma is currently serving as the Co-Editor-in-Chief for the IEEE TRANSACTION ON INDUSTRY APPLICATIONS, an Associate Editor for two IEEE transaction journals, and the Vice Chair for two IEEE technical committees. He was the recipient of the "Excellent Young Wind Doctor Award" by the European Academy of Wind Energy, the "Outstanding Youth Award" by the China Power Supply Society, and several prized paper awards by IEEE.

Quan Zhong received the B.Sc. degree in electrical engineering from Wuhan University, Wuhan, China, in 2021. He is currently working toward the M.Sc. degree with Shanghai Jiao Tong University, Shanghai, China.

His research interests include health monitoring and reliability analysis of power semiconductor devices.